https://doi.org/10.5194/hess-2023-253
Preprint. Discussion started: 14 December 2023

Hydrology and Earth System Sciences Discussions

Estimating flood discharge at river bridges using the entropy theory. Insights from Computational Fluid Dynamics flow fields

Farhad Bahmanpouri[1†], Tommaso Lazzarin[2†], Silvia Barbetta[1], Tommaso Moramarco[1], Daniele P. Viero[2]

[1]Research Institute for Geo-Hydrological Protection, National Research Council (CNR), Perugia, 06128, Italy
[2]Department of Civil, Environmental and Architectural Engineering, University of Padova, 35131, Italy

† F.B. and T.L. equally contributed to the study.

Correspondence to: Daniele P. Viero (daniele.viero@unipd.it)

Abstract. Estimating the flow velocity and discharge in rivers is of particular interest for monitoring, modelling, and research purposes. Instruments for measuring water level and surface velocity are generally mounted on bridge decks, and this poses a challenge because the bridge structure (e.g., piers and abutments) can lead to perturbated flow fields. The current research aims to investigate the applicability of the entropy theory to estimate the velocity distribution and the discharge in the vicinity of river bridges. To this purpose, a Computational Fluid Dynamics (CFD) model is used to obtain three-dimensional flow fields along a stretch of the Paglia River (central Italy), where a historical multi-arch bridge strongly affects flood flows. The input data for the entropy model include the cross-sectional bathymetry and the surface velocity provided by the numerical simulations. Different flow conditions and cross-sections, either upstream and downstream of the bridge, are considered. It is found that the entropy model can be applied safely upstream of the bridge, also when forced with a single (i.e., the maximum) value of the surface velocity, with errors on total discharge below 13% in the considered case. On the contrary, downstream the bridge, the wakes generated by the bridge piers strongly affect the velocity distribution, both in the spanwise and in the vertical directions, and for very long distances. Here, notwithstanding the complex and multimodal spanwise distribution of flow velocity, the entropy model estimates the discharge with error lower than 8% if forced with the river-wide distribution of the surface velocity. The present study has important implications for the optimal positioning of sensors and suggest the potential of using CFD modelling and entropy theory jointly to foster the knowledge of river systems.

1 Introduction

Velocity and discharge measurements in rivers are fundamental for monitoring, modelling, and research purposes (Depetris, 2021; Di Baldassarre and Montanari, 2009; Dottori et al., 2013; Gore and Banning, 2017; Herschy, 2009). Unfortunately, measuring river discharge can be very challenging due to different reasons, for example in the case of intermittent rivers typical of semi-arid regions, of flash floods in mountain areas, of flood flows involving wide floodplains, of freshwater flows affected by saline tidal intrusions in estuaries, etc. Traditional methods of measuring flow characteristics are generally expensive, time-consuming, and risky for operators, mainly during severe flow conditions, and they are not feasible in remote and inaccessible locations.

In natural rivers with large cross-sections, the streamwise velocity typically shows a logarithmic vertical distribution due to the bottom roughness. According to field data, the maximum velocity is found just below the free surface and gradually decreases towards the bed (Franca et al., 2008; Guo, 2014). However, plenty of factors contributes in making the velocity distribution irregular. For instance, channel bends and deformed bathymetry produce large-scale secondary currents (Constantinescu et al., 2011; Lazzarin and Viero, 2023; Yang et al., 2012), and the presence of banks and of discontinuities of bed elevation in the spanwise directions can generate secondary currents of the second kind (Nikora and Roy, 2011; Proust and Nikora, 2020), which all increase the three-dimensionality of the flow field and alter the vertical and spanwise distribution of the flow velocity.

The presence of in-stream structures such as bridges, that are characterized by the presence of piers and/or of lateral abutments, can induce significant alterations on the flow field (Laursen, 1963, 1960), producing complex and rapidly varying flow patterns, with the formation of strong three dimensional flow structures (Ataie-Ashtiani and Aslani-Kordkandi, 2012; Chang et al., 2013; Salaheldin et al., 2004). Secondary currents in the cross-section transport low momentum fluid from lateral region to the center of the channel, and high-momentum fluids from the free surface toward the bed (Bonakdari et al., 2008; Nezu and Nakagawa, 1993; Yang et al., 2004). This creates systems of vortices with horizontal (horseshoe vortex) or vertical axes (wake vortex) that in turn modify the velocity distribution (Kirkil and Constantinescu, 2015; Sumer et al., 1997). The wakes generated by in-stream obstacles and contractions can propagate downstream of bridges for quite long distances (Briaud et al., 2009; Yang et al., 2021).

The cross-sectional velocity distribution at bridges is of particular interest in hydrology and hydraulics. Indeed, measuring instruments such as hydrometers, as well as radar sensors or cameras for estimating the surface velocity, are generally mounted on bridge decks for convenience reasons. Notwithstanding the recommendation of installing height gage at the upstream side of bridges (Meals and Dressing, 2008), measuring instruments are often located downstream of bridges, which is expected to complicate the discharge estimate (Kästner et al., 2018).

Besides the measurement of the flow discharge, the knowledge of flow field nearby bridges has additional practical implications; the flow velocity is the dominant parameter to study the local scour at a bridge pier, which may result in being responsible for the bridge collapse in some extreme conditions (Barbetta et al., 2017; Federico et al., 2003; Lu et al., 2022). The formation of scours at piers and abutments can be attributed to a significant extent to the flow patterns produced at their immediate vicinity, such as the flow contraction and the large-scale turbulent structures (Cheng et al., 2018; Khosronejad et al., 2012).

While monitoring river discharge on the ground has definite advantages (Fekete et al., 2012), the use of traditional methods (e.g., current meters, ADCPs) is not straightforward in case of high-flow conditions. Alternative methods have been proposed to estimate the velocity distributions and the flow discharge through indirect approaches (Bogning et al., 2018; Fekete and Vörösmarty, 2002; Spada et al., 2017; Vandaele et al., 2023; Zhang et al., 2019). These methods typically make use of some field data, whose measurements is generally relatively easy, to reconstruct the entire cross-sectional distributions. Some of this data include the water level and the velocity at the free surface, which can be collected by permanent measurement stations mounted on bridge decks and based on a number of diverse techniques (e.g., Eltner et al., 2020; Herschy, 2009; Jodeau et al., 2008; Schweitzer and Cowen, 2021).

One of the most promising methods to exploit joint measures of water level and surface velocity is based on the entropy concept. Researchers have widely applied this concept to predict velocity distributions as well as other relevant parameters in open channels (Bonakdari et al., 2015; Chiu, 1989; Chiu and Said, 1995; Chiu et al., 2005; Ebtehaj et al., 2018; Moramarco and Singh, 2010; Singh et al., 2017; Sterling and Knight, 2002; Termini and Moramarco, 2017). Termini and Moramarco (2020) identified the cross-sectional velocity by applying the entropy concept and by testing the spatial distribution of the entropic parameter, M, along with the location of the velocity dip. Using a one-dimensional flood routing model and an entropy velocity profile, Abdolvandi et al. (2021) developed a novel conversion factor estimation procedure. Using two different assumptions, they estimated discharge at weak gauging sites; constant velocity factor and aspect ratio-related velocity factor. Based on a picture-based technique, Chahrour et al. (2021) measured the discharge of the Isère River at Grenoble University Campus using the entropy-based approach. A particle tracking velocimetry (PTV) approach was used to estimate surface velocities from video images, which were then used to calculate entropy. Using point velocity data collected at $0.6\,D$ depth from the surface of the water (being D the total water depth), Vyas et al. (2021) examined the entropy concept. A correlation was established between the maximum point-velocity based on the sectional mean flow velocity and the maximum point-velocity estimated at $0.6\,D$ depth. Using ADCP surface velocity measurements at different cross-sections, Bahmanpouri et al. (2022a) applied the entropy approach at the confluence of large rivers (Negro and Solimões rivers); despite the complex hydrodynamic settings, the entropy method well predicted the velocity field and the flow discharge. Ammari et al. (2022) applied the entropy concept to derive the discharge rate based on the estimate of a single parameter for the drainage network of a wide region of the central and east part of Algeria. Their outputs suggested a smooth spatial distribution of the entropy parameter along channels, associated to reliable discharge estimations. Bahmanpouri et al. (2022b), based on only one surface velocity measurement provided by an unmanned aerial vehicle (UAV), estimated the cross-sectional velocity and the discharge (with errors lower than 13%) along two European rivers.

All these studies demonstrated the accuracy of the entropy method referring to undisturbed flow conditions, or to cases like confluences or low curvature bends characterized by large-scale three-dimensional effects and secondary currents. However, in practical applications, water levels and free-surface velocities are often measured by instruments mounted on bridge decks. In this case, the vicinity of structures such as bridge piers and abutments can produce flow contraction, separation, and turbulent wakes, generally associated with abrupt variations in the local flow field and deformed cross-sectional distribution of the flow velocity.

Accordingly, the present research is meant to investigate the predictive ability of the entropy theory in estimating the velocity distribution, and hence the streamflow discharge, in the case of complex flow fields generated by the presence of a bridge. We choose a reach of the Paglia River, in the central Italy, as a relevant case study; here, a level gauge and a radar for

https://doi.org/10.5194/hess-2023-253
Preprint. Discussion started: 14 December 2023

Hydrology and Earth System Sciences
Open Access
Discussions

measuring the surface velocity are mounted on a historical multi-arch bridge, which produces strong flow-structure interactions. A physics-based, three-dimensional Computational Fluid Dynamics model is used to provide complete and accurate velocity distributions, both upstream and downstream of the bridge section, which are compared with those obtained using the entropy theory forced with different input data. Guidelines for the proper application of the entropy theory, and the optimal choice and positioning of measuring instruments are finally given.

2 Material and Methods

2.1 Field Site

The Paglia river, in the central part of Italy (Figure 1a), is a tributary of Tiber River, subjected to severe flooding and high sediment transport. The reach of interest is across the Adunata bridge (Figure 1b), near the town of Orvieto, where the Paglia river subtends a basin area of about 1’200 km². Here, the average discharge is of 10 m³/s; however, flood discharge can reach estimated values of up to 2’500 m³/s.

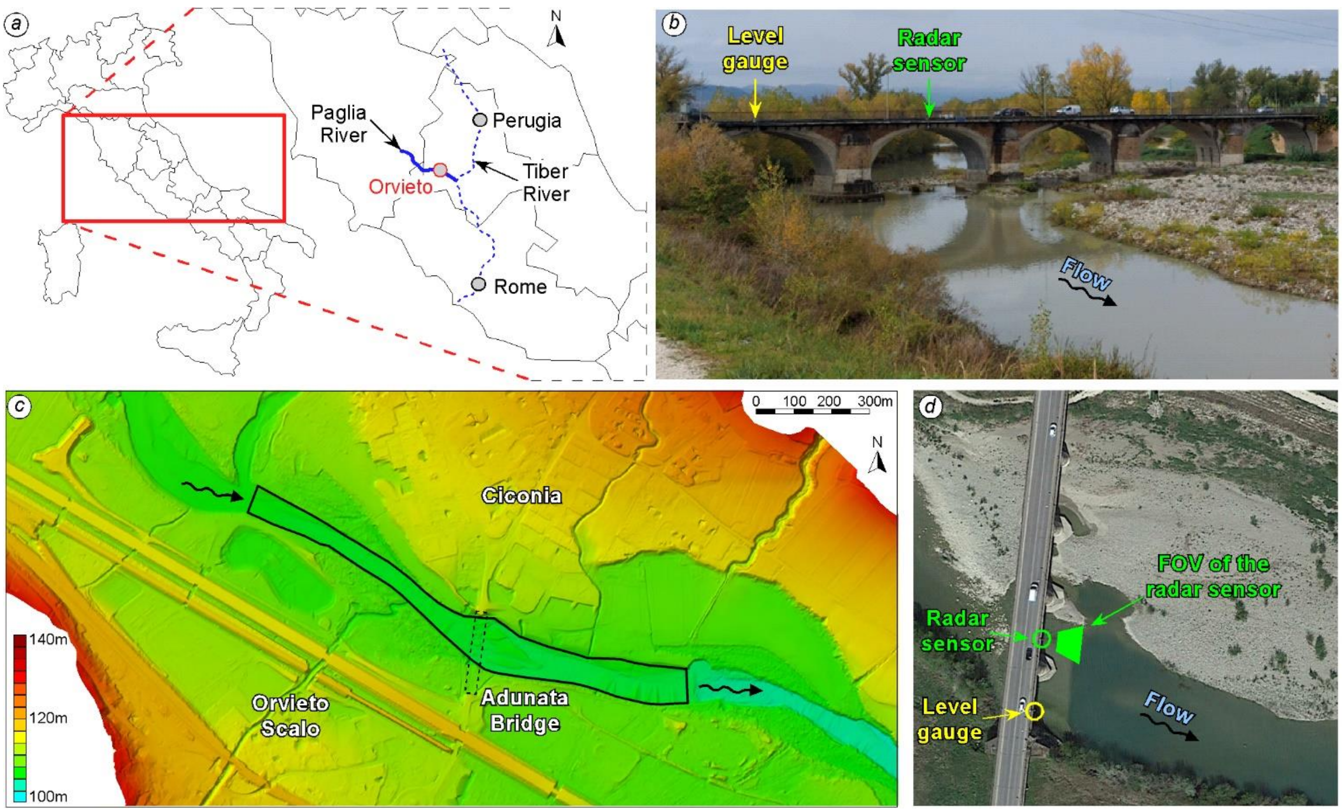

Figure 1. a) Location of the field site; b) downstream view of the Adunata bridge on the Paglia river during normal flow condition (11.11.2021); c) Digital Terrain Model (DTM) nearby the Adunata bridge (dotted line), with the domain of the 3D CFD model (black line); d) location of the level gauge and of the radar sensor with the field of view (FOV) on aerial image (© Google Earth).

https://doi.org/10.5194/hess-2023-253
Preprint. Discussion started: 14 December 2023

Hydrology and Earth System Sciences Discussions

The Adunata bridge connects the settlements of Orvieto Scalo and Ciconia, as part of the Italian State Road n.71 (Figure 1c). It is a masonry multi-arch bridge, with 5 arches ending at four piers on the river bed. On the right-hand side, an abutment sustains the bridge and separates it from the floodplain; on the left-hand side, the bridge deck is supported by the main levee. Close to the bottom, the piers have a roughly elliptical shape with the mayor axis, aligned with the flow, 15 m long, and the minor axis, orthogonal to the flow, 5.7 m wide. At the bottom, each pier is sustained by an elliptical plinth whose profile is 2.0 m larger than the pier. The center-distance between the piers is 23.2 m. The piers width increases approaching the deck because of the arches; the deck width is approximatively 10 m.

The main thread of the flow is at the right-hand side of the river, and a large depositional area forms on the left-hand side just downstream of the bridge (Figure 1b). The main channel axis is characterized by a significant curvature, bending to the left at the bridge section (Figure 1c).

2.2 Available Data

In the downstream side of the Adunata Bridge, a water level gauge is placed at the center of the first arch, and a radar sensor for measuring the water surface velocity is located at the second arch (Figure 1d). The field of view (FOV) of the radar sensor is also shown in Figure 1d. The time resolution of both the sensors is 10 min.

In addition, a number of flowrate measures and cross-sectional velocity distributions are provided by the Umbria Region Hydrological Service. The flowrate data were collected using a current meter a few tens of meters downstream of the Adunata Bridge, by wading in the period 2009-2011 (flowrate ranging between 3.3 and 14.3 m^3/s), and from the bridge in the period 1995-2010 (flowrate ranging between 16.8 and 147 m^3/s); additional flowrate data were collected using an Acoustic-Doppler Current Profiler (ADCP) some hundreds of meters upstream of the bridge in the period 2014-2019 (flowrate ranging between 0.37 and 45 m^3/s). The official rating curve for the Adunata Bridge, provided by ARPA Lazio, is based on these measures.

As detailed in the following sections, the rating curve, the water levels, and the free-surface velocity data collected by the two sensors, are used to validate the numerical models; the cross-sectional velocity distributions measured with the ADCP are used to further assess the entropy-based velocity distributions.

2.3 Numerical Model

The commercial CFD software STAR-CCM+ (Siemens) is used for the numerical simulations. It implements the Finite Volume method to compute the flow field on unstructured, Cartesian computational grids. In the present application, the two-phase Volume of Fluid (VoF) method is used to distinguish water and air in the computational domain (Hirt and Nichols, 1981). This method was shown to well capture the water surface in complex open channel flows (Horna-Munoz and Constantinescu, 2018; Lazzarin et al., 2023b; Li and Zhang, 2022; Luo et al., 2018; Yoshimura and Fujita, 2020).

In the used setup, the model solves the Reynolds-Averaged Navier-Stokes (RANS) equations, in which the stress tensor in the momentum equations is related to the mean flow quantities by adopting the Bousinnesq approximation. The eddy viscosity, μ_T, is determined by solving transport equations for the turbulent kinetic energy, k, and dissipation rate, ε, according to the realizable k-ε turbulence model (Shih et al., 1995), which was shown to provide reliable predictions for large-scale complex flows in natural rivers (e.g., Horna-Munoz and Constantinescu, 2018).

The simulations are advanced in time with an implicit, 1st order discretization, until reaching steady state conditions. The computational domain reproduces a ~1'100 m long reach of the Paglia River (Figure 1c), centered at the Adunata bridge. The average size of the grid elements is of 1.0 m. Starting 100 m upstream of the bridge and up to 300 m downstream of the bridge, the grid is refined using elements with average length 0.5 m. To well capture the near-wall boundary layer, a prism layer refinement with three layers is used to reduce the wall-normal thickness of the grid cells close to solid boundaries (i.e., the riverbed and bridge structure). The final computational grid is made of ~4 million elements.

A rough-wall, no-slip condition is imposed at the solid boundaries by means of a wall function (roughness height of 0.1 m at the bottom, and of 0.01 m at the bridge surfaces). The upper boundary of the computational grid is treated as a symmetry plane (i.e., slip-condition) for the air-flow. The water elevation at the outlet (i.e., downstream section) is kept fixed in time by imposing a suitable hydrostatic-pressure distribution. The value of the downstream level, for each of the simulated scenarios, is derived from an auxiliary two-dimensional (2D), depth-averaged hydrodynamic model calibrated on available data; the 2DEF model has been used to this purpose (see Appendix A for details on the model and its calibration/verification). A constant-in-time, logarithmic velocity distribution is imposed as upstream boundary condition for the water fraction. For the air fraction (upper part of the numerical domain), zero velocity and zero pressure are imposed at the inlet and at the outlet, respectively.

The 3D-CFD model is validated by comparing the surface velocity computed by the model with those measured by the radar sensor located downstream of the bridge (see the yellow bullets in Fig. A2c,d, in the Appendix A).

2.4 Flood events considered in the study

Three different steady flow conditions are simulated with the 3D-CFD model STAR-CCM+, which correspond to the peak flow conditions of flood events occurred in 2012, 2019, and 2022 (Table 1). During the most severe flood of 2012, water flowed also through the floodplains adjacent to the main river channel. The preliminary simulation carried out with the 2DEF depth-averaged model showed that 700 m³/s flowed through the floodplain, overflowing the bridge access roads, and 1800 m³/s flowed within the main channel; this last value is used in the 3D-CFD simulation, which considers only the main channel of the river. The flood events of 2019 and 2022, although being quite ordinary, were the largest floods occurred after the installation of the radar sensor for the surface velocity data (surface velocity data are not available for the 2012 flood).

Event	Discharge [m³/s]
2012	1800 (2500)
2019	450
2022	160

Table 1. Simulations performed in the present work. The value in brackets indicate the total discharge considering also the flow over floodplains, not considered in the 3D simulations.

https://doi.org/10.5194/hess-2023-253
Preprint. Discussion started: 14 December 2023

Hydrology and Earth System Sciences
Open Access
EGU
Discussions

2.5 Entropy theory

Chiu (1989) developed an estimation of cross-sectional velocity distribution, $U(x,y)$, using the entropy probability density function. Later, Moramarco et al. (2004) simplified the estimation. Using this approach, one can determine the entropy-based velocity profile along the verticals as follows:

$$U(x_i, y) = \frac{U_{max\,v}(x_i)}{M} \ln\left[1 + (e^M - 1)\frac{y}{D(x_i) - h(x_i)} \exp\left(1 - \frac{y}{D(x_i) - h(x_i)}\right)\right] \quad i = 1 \dots N_v \tag{1}$$

where U is the time-averaged velocity, $U_{\max\,v}(x_i)$ is the maximum value of U along the i^{th} vertical, x_i is the distance of the i^{th} sampled vertical from the left bank, $h(x_i)$ is the dip, i.e., the depth of $U_{\max\,v}(x_i)$ below the water surface, $D(x_i)$ the flow depth, y is the distance of the velocity point from the bed, and N_v is the number of verticals sampled across the river section. M can be estimated using the linear entropic relation using the mean and the maximum flow velocity, U_m and U_{max}, measured within the entire cross-section (Chiu, 1989):

$$U_m = \left(\frac{e^M}{e^M - 1} - \frac{1}{M}\right) U_{max} = \phi(M)\, U_{max} \tag{2}$$

In general, for a given river site, $\phi(M)$ is assumed to be constant for all flow conditions, while for ungauged sites $\phi(M)$ can be estimated as (Moramarco and Singh, 2010):

$$\phi(M) = \frac{\frac{1}{n} R^{1/6}}{\sqrt{g}\,\frac{1}{k}\left[\ln\left(\frac{y_{max}}{y_o}\right) + \frac{h}{y_{max}} \ln\left(\frac{h}{D}\right)\right]} \tag{3}$$

where y_{max} is the location of U_{max} from the bottom and y_o is the datum where the velocity is equal to zero, k is the von Karman constant, R is the hydraulic radius, n is the Manning roughness and D is the maximum flow depth.

Whether at a river site only the surface velocities, $U_{surf}(x_i, D(x_i))$ are available, then $U_{\max\,v}(x_i)$ can be estimated as (Fulton and Ostrowski, 2008):

$$U_{max\,v}(x_i) = \frac{U_{surf}(x_i, D(x_i))}{\frac{1}{M}\ln[1 + (e^M - 1)\delta(x_i) e^{1-\delta(x_i)}]} \tag{4}$$

where $\delta(x_i) = D(x_i)/[D(x_i) - h(x_i)]$. Specifically, if $h(x_i) = 0$, it follows that $\delta(x_i) = 1$ and, hence, $U_{maxv}(x_i) = U_{surf}(x_i, D(x_i))$. The magnitude of $\delta(x_i)$ can be obtained based on the iterative procedure proposed by Moramarco et al. (2017). The procedure can be applied for sites with a given $\phi(M)$. The procedure is based on assigning an initial dip, $h(x_{i,p=1})$, where the maximum surface velocity occurs (p is the iteration).

For the current research, according to the initial value of dip, a laboratory distribution law of dip suggested by Yang et al. (2004) is implemented, and the $U_{maxv}(x_{i,p=1})$ is assessed by Eq. (4) for all the considered verticals. $U_{max(p=1)}$ is identified as the maximum of $U_{maxv}(x_{i,p=1})$. Therefore, once $U_{maxv}(x_{i,p=1})$ is replaced in Eq.(1), it enables estimation of the depth-averaged velocities in each cross-section. For the first iteration, the mean flow velocity, $U_{m(p=1)}$, can be estimated using the velocity-area method. As a consequence, $\phi(M_{com,p=1})$ can be computed by Eq.(2), using $U_{m(p=1)}$ and $U_{max(p=1)}$. The iteration continues

https://doi.org/10.5194/hess-2023-253
Preprint. Discussion started: 14 December 2023

until the error of $\phi(M_{com,p}) - \phi(M)$ becomes lower than 0.01. For more details, the reader is referred to Moramarco et al. (2017).

3 Results and discussions

The comparison between the entropy-based and the CFD-derived velocity distributions is performed considering four cross-sections (Figure 2), at a distance of 50 m upstream and 50, 100, and 200 m downstream of the bridge, and the three flood events of 2012, 2019, and 2022 (see Table 1).

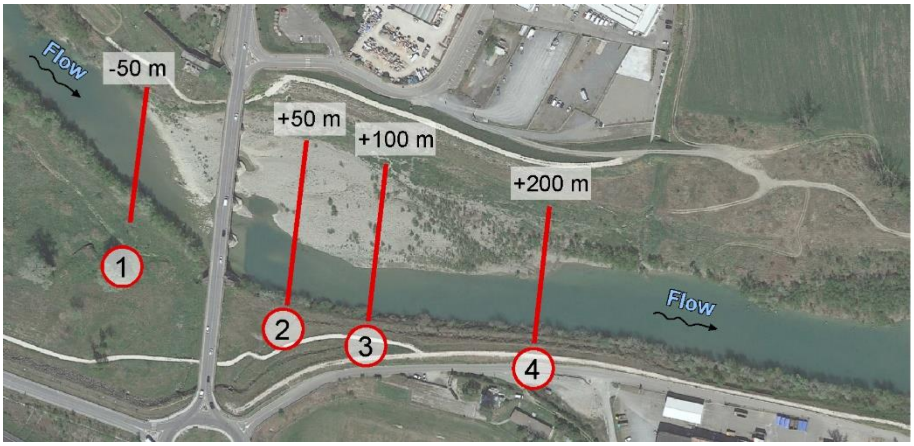

Figure 2. Location of the Adunata Bridge and of the four selected cross-sections (aerial image from © Google Earth).

First, the study analyzes the variability of the entropy parameter, $\phi(M)$, at the four cross-sections, as derived from the cross-sectional velocity distributions provided by both the 3D-CFD model and the ADCP measures (Sect. 3.1). Then, in applying the entropy model to estimate the cross-sectional velocity, two different procedures are considered. In the first one, the entropy model is forced with the river-wide distribution of the surface velocities computed by the 3D-CFD model (this is described in the following Sect. 3.2); in the second one, only the maximum value of the surface velocity computed by the 3D-CFD model is considered as input for the entropy model (Sect. 3.3). The first procedure is applied to all the four cross-sections, whereas the latter is only applied to cross-sections 1 and 4, i.e., where the effects of the bridge piers is minimal so that the spanwise velocity distribution is unimodal.

3.1 Variability of the entropy parameter

Some relevant parameters that characterize the flow field (e.g., aspect ratio, average and maximum velocity) at the selected cross-sections are presented in Table 2 for the peak flow condition of the three flood events.

https://doi.org/10.5194/hess-2023-253
Preprint. Discussion started: 14 December 2023

Hydrology and Earth System Sciences
Discussions

Year	Distance from the bridge (m)	Channel aspect ratio (width/depth)	Average Velocity (m/s)	Maximum Velocity (m/s)	$\phi(M)$	M
2012	−50	9.26	4.43	6.82	0.650	1.91
	+50	13.78	2.91	7.01	0.415	−1.03
	+100	11.05	3.61	6.68	0.541	0.50
	+200	8.5	4.06	5.48	0.740	3.4
2019	−50	16.3	3.0	4.21	0.711	2.87
	+50	18.45	1.93	3.74	0.515	0.18
	+100	14.75	2.08	3.26	0.639	1.75
	+200	12.84	2.40	3.47	0.690	2.51
2022	−50	27.7	2.57	3.40	0.755	3.71
	+50	27.3	1.33	2.58	0.514	0.17
	+100	20.9	1.55	2.19	0.711	2.86
	+200	13.23	1.97	2.56	0.767	3.96

Table 2. Entropy parameter, $\phi(M)$, and other relevant flow data for the cross-section of Figure 2 and the three considered flood events of Table 1.

Since the entropy parameter is typically assumed to be constant for all flow conditions at a given cross-section, it is of interest to analyze its actual variation by exploiting the flow fields provided by the 3D-CFD model. The values of $\phi(M)$ reported in Table 2 are plotted in Figure 3 as a function of the downstream distance from the bridge. At the first cross-section downstream of the bridge (i.e., cross-section 2), although referring to different flow conditions, the entropy parameters computed with the 3D-CFD and the current meter velocity distributions show the same magnitude, further confirming the reliability of the 3D-CFD model.

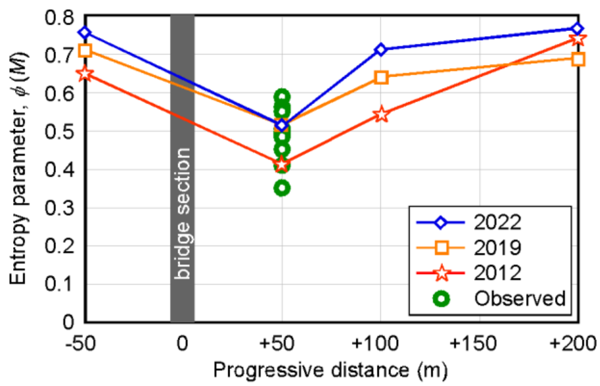

Figure 3. Entropic parameter $\phi(M)$ as a function of the distance from the bridge (positive downstream), computed from the 3D-CFD flow fields of the different simulated scenarios; green dots refers to data derived from ADCP field measures.

For each flood event, at cross-sections 1 and 4, i.e., where the flow field is not characterized by the wakes generated by the bridge piers, the entropic parameter assumes similar values, which can be identified as "undisturbed" values. The variability of such undisturbed values of $\phi(M)$ with the flowrate is relatively small, as all the values fall in the range

https://doi.org/10.5194/hess-2023-253
Preprint. Discussion started: 14 December 2023

$0.65 < \phi(M) < 0.75$, which is in agreement with the range found by Bahmanpouri et al. (2022b) for similar European rivers. On the contrary, at cross-sections 2 and 3, just downstream of the bridge, the values of $\phi(M)$ are consistently reduced due to the effect of the bridge. For the moderate peak flow of the 2022 event, the entropy parameter recovers undisturbed values already at cross-section 3, i.e., 100 m downstream of the bridge. In the largest flood event of 2012, which produced near pressure-flow conditions at the bridge with marked localized increasing of the flow velocity, $\phi(M)$ decreases from 0.64 to 0.42, and a sensible reduction is still present 100 m downstream of the bridge (cross-section 3).

This first analysis suggests that assuming constant values of $\phi(M)$ can be reasonable in undisturbed river reaches; however, in case of irregular flow fields induced by the interactions with in-stream structures, the entropy parameter $\phi(M)$ can vary with respect to undisturbed values and, in addition, it can show substantial variations with the flowrate.

3.2 Entropy model forced with the river-wide profile of free-surface velocity

The efficacy of the entropy model is here tested for the case in which the surface velocity is known for all the width of the cross-section. This could be the case in which the river-wide surface velocity is estimated from imaging techniques (e.g., Eltner et al., 2020; Schweitzer and Cowen, 2021). The results, in terms of cross-sectional velocity distributions, are presented for brevity only for the intermediate peak flow of the 2019 flood event, and for the most challenging cross-sections just downstream of the bridge, where the flow field is disturbed by the pier wakes. The same results, for the peak flows of 2012 and 2022 events, are provided as supplementary material.

Figure 4 presents the cross-sectional velocity distribution 50 m downstream of the bridge (cross-section 2). As shown by the 3D-CFD flow field (Fig. 4a) and reflected in the low value of $\phi(M)$ for this cross-section (Table 2 and Figure 3), the effect of the piers is very strong, such that there is a clearly uneven distribution of the cross-sectional velocity because of the wakes developing downstream the piers. Despite that, using as input the river-wide distribution of the surface velocity provided by the CFD simulation, the entropy model can reliably capture the salient features of the cross-sectional velocity distribution.

Figure 4(c-e) highlights the comparison of 3D-CFD and entropy flow velocities along three verticals located at 0.2 B, 0.5 B, and 0.8 B (where B is the channel width). Compared to the results of the 3D-CFD model, the entropy approach underestimates the velocity close to the bed. Just downstream of the bridge, due to the presence of the bridge arches, the flow field provided by the 3D-CFD model is configured as a sort of partial orifice flow that increases the vertical uniformity of the velocity distribution compared to a uniform shear flow. Of course, the entropy model cannot capture such a localized flow features, which entails some difference in the patchiness of the physics-based and the entropy velocity distributions (Figure 4a-e). Since the velocities and the volumetric fluxes are still relatively small near the bed, these discrepancies marginally affect the estimation of the section-averaged velocity and, consequently, of the total discharge (Table 3). The percentage error is quite larger (7.6%) for the very high-flow condition of the 2012 event (see Supplementary Materials), due to the accentuation of orifice-flow conditions associated to the higher water levels.

https://doi.org/10.5194/hess-2023-253
Preprint. Discussion started: 14 December 2023

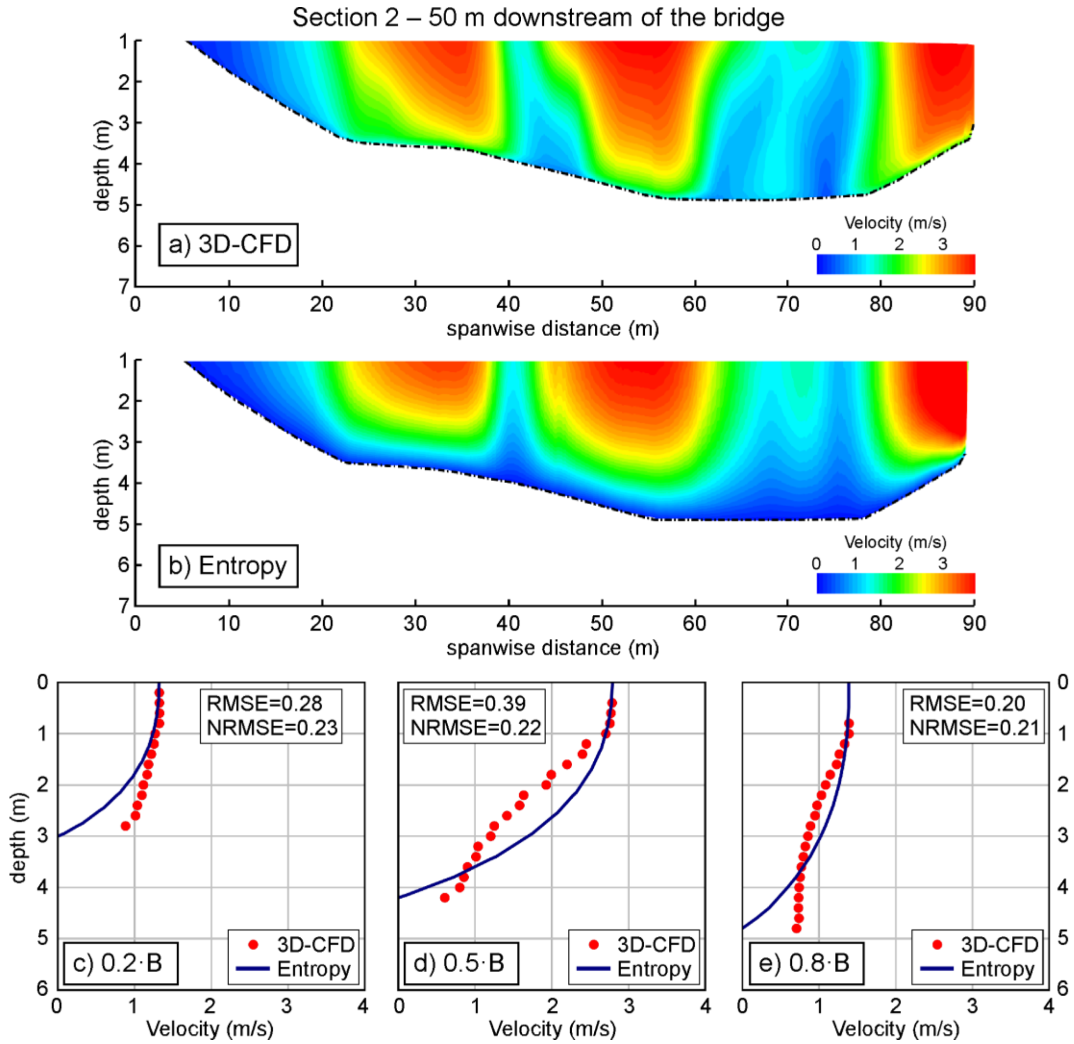

265 **Figure 4. Flood event of 2019, cross-section 2 (50 m downstream of the bridge). Velocity distributions provided by (a) the 3D-CFD model, and (b) the entropy model forced with the river-wide distribution of the free-surface velocity. Comparison of vertical distributions of velocity at 0.2*B* (c), 0.5*B* (d), and 0.8*B* (e), where *B* is the width of the cross-section.**

Figure 5 depicts the cross-sectional velocity distributions at a larger distance from the bridge, i.e. at cross-section 3, placed 100 m downstream the bridge. The visual comparison with Figure 4 suggests that the effects of the piers on the flow field are reduced because of the increased distance, and the cross-sectional distribution provided by the 3D-CFD model (Figure 5a) appears more regular. The statistical analysis confirms that in this case the entropy model (Figure 5b) is able to simulate the velocity profiles with a higher accuracy.

Hydrology and Earth System Sciences
Discussions

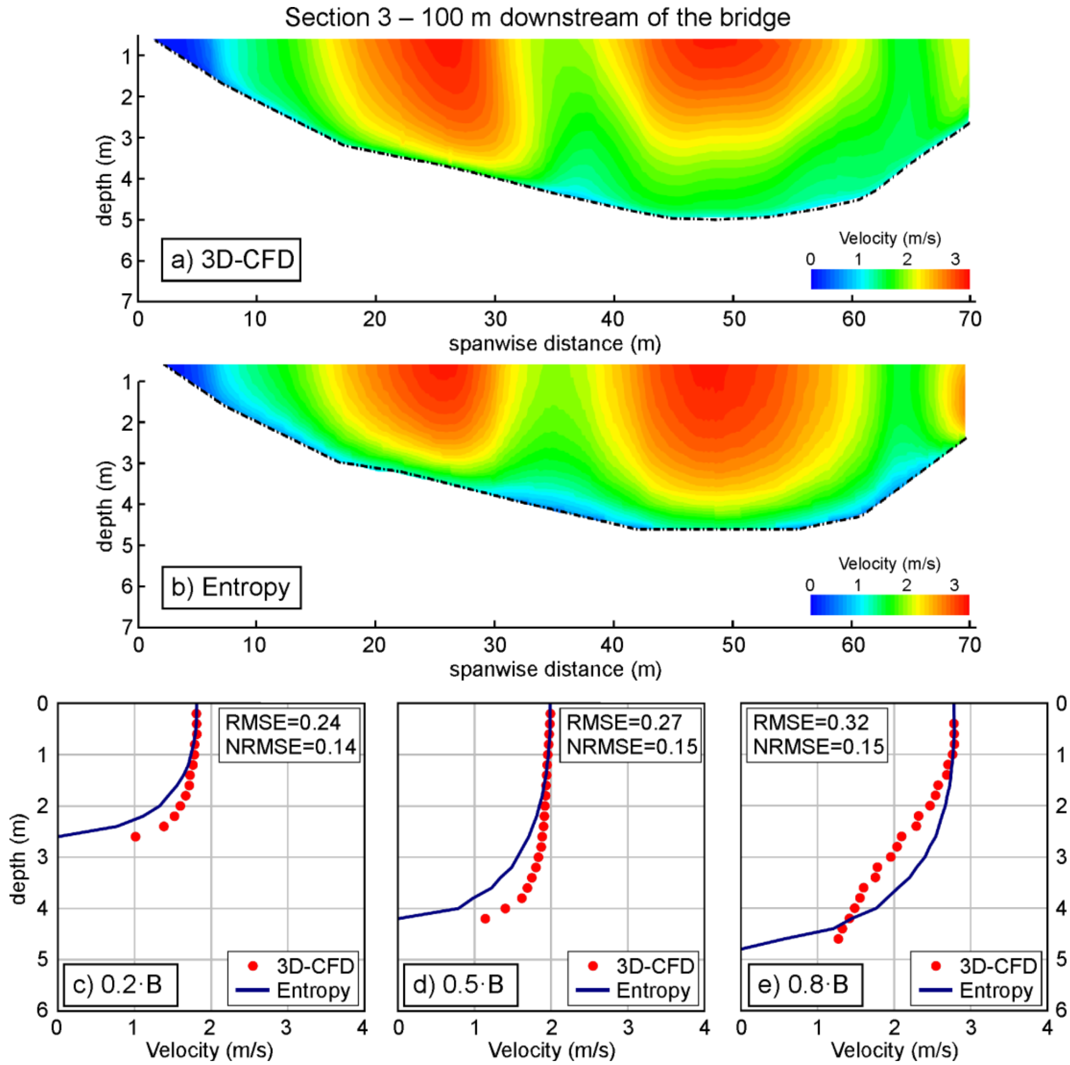

275 **Figure 5. Flood event of 2019, cross-section 3 (100 m downstream of the bridge). Velocity distributions provided by (a) the 3D-CFD model, and (b) the entropy model forced with the river-wide distribution of the free-surface velocity. Comparison of vertical distributions of velocity at 0.2*B* (c), 0.5*B* (d), and 0.8*B* (e), where *B* is the width of the cross-section.**

Figure 6 shows the cross-sectional velocity distributions of 3D-CFD and entropy models for the cross-section 4, i.e. 200 m downstream of the bridge. Compared to cross-section 3, the effect of the bridge piers is further reduced, because of both the distance and the more compact shape of the cross-section. Since the effect of the bridge piers is minimum, the statistical analysis shows a better agreement of the entropy model results with the CFD-based data. Though areas with high velocities are still visible in simulations with higher values of the discharge (i.e., events of 2012 and 2019), for the high-flow conditions of 2022, the effect of the bridge pier has completely vanished. Therefore, the lower the flow discharge the lower the distance from the bridge to reach the normal flow condition without the bridge effect.

https://doi.org/10.5194/hess-2023-253
Preprint. Discussion started: 14 December 2023

Hydrology and Earth System Sciences
Discussions

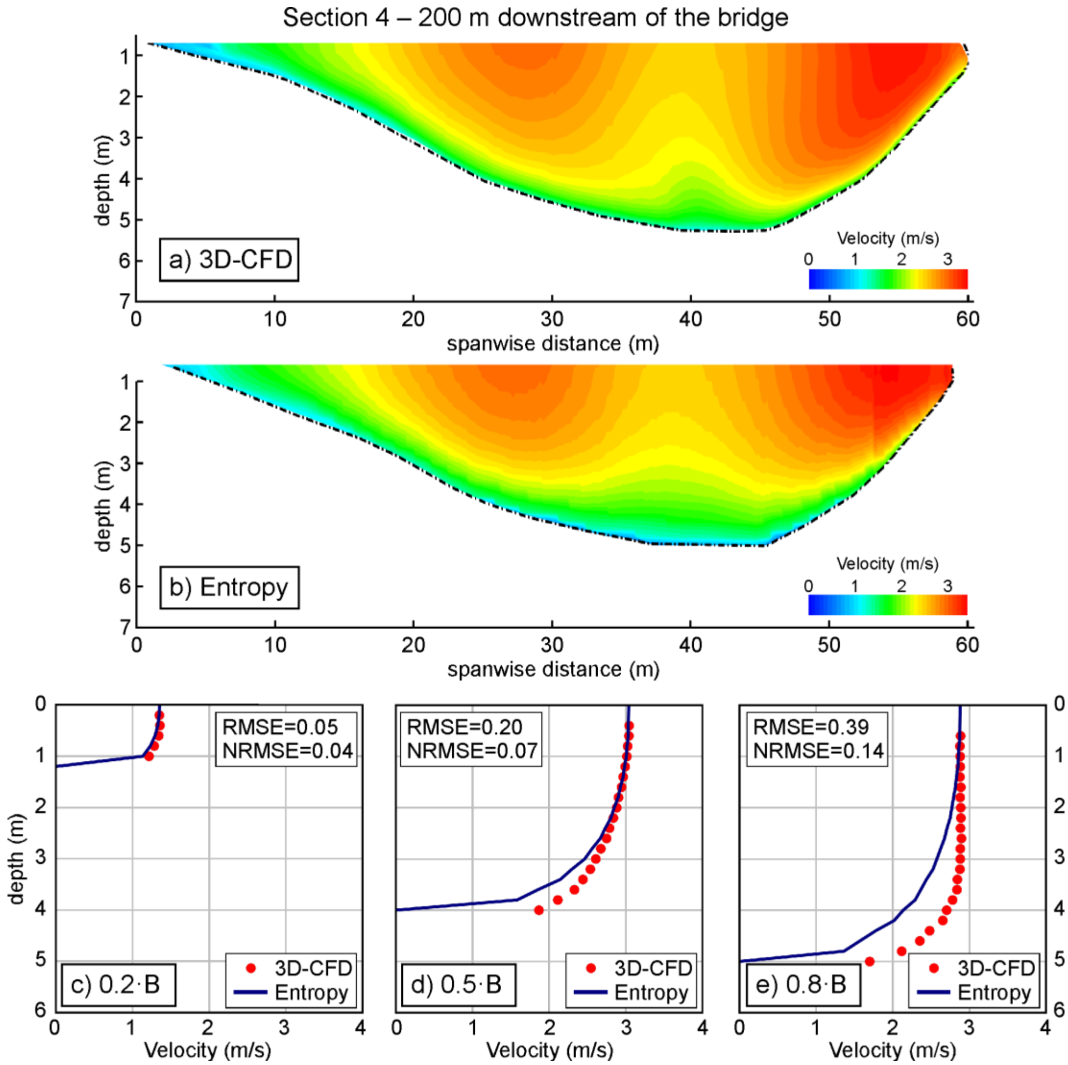

285 **Figure 6. Flood event of 2019, cross-section 4 (200 m downstream of the bridge). Velocity distributions provided by (a) the 3D-CFD model, and (b) the entropy model forced with the river-wide distribution of the free-surface velocity. Comparison of vertical distributions of velocity at 0.2*B* (c), 0.5*B* (d), and 0.8*B* (e), where *B* is the width of the cross-section.**

The results here presented show that, when the river-wide distribution of the free-surface velocity is provided, the entropy method allows to provide good estimations of the cross-sectional velocity distribution even when the influence of bridge piers, and thus the unevenness of the flow field, is relevant. The main discrepancies are observed in the regions of flow with low values of velocity, which slightly affect the estimation of the flow discharge. Table 3 lists some statistics and error percentages for the depth-averaged velocity and discharge estimates for all cross-section and the three events considered. The estimation provided by the entropy method are in good agreement with results of CFD model, both upstream and downstream of the Adunata bridge. Though the precision is slightly reduced downstream of the bridge, the results are reliable also in the vicinity of the structure (i.e., at cross-section 2), suggesting the applicability of the entropy model to

https://doi.org/10.5194/hess-2023-253
Preprint. Discussion started: 14 December 2023

Hydrology and Earth System Sciences
Discussions

estimate the flow discharges even in case of irregular distributions of the cross-sectional velocity, provided that the river-wide distribution of the surface velocity is used as input data.

Flood event	Cross-section	Distance from the bridge (m)	Average velocity (m/s)		Discharge (m^3/s)		Error percentage (%)
			3D-CFD	Entropy	3D-CFD	Entropy	
2012	1	−50	4.43	4.64	1’800	1’885	+4.7
	2	+50	2.91	2.69		1’664	−7.6
	3	+100	3.61	3.54		1’765	−2.0
	4	+200	4.06	4.30		1’906	+5.9
2019	1	−50	3.0	3.0	450	450	+0.1
	2	+50	1.93	1.90		443	−1.5
	3	+100	2.08	2.12		459	+2.0
	4	+200	2.40	2.54		476	+5.8
2022	1	−50	2.55	2.66	160	166	+3.7
	2	+50	1.32	1.24		150	−6.3
	3	+100	1.55	1.51		157	−1.9
	4	+200	1.97	1.98		161	+0.6

Table 3. Flood event of 2019. Comparison between 3D-CFD outputs and entropy-based estimations forced with the river-wide distribution of the free-surface velocity.

3.3 Entropy model forced with a single value of free-surface velocity

In this section, the results are presented considering only a single value of the surface velocity as input for the entropy model, which corresponds to the maximum surface velocity predicted by the 3D-CFD model. Two different spanwise velocity distributions are enforced in the entropic model, namely a parabolic spanwise distribution (PSD) and an elliptic spanwise distribution (ESD). Of course, applying the entropy model using a unique value of the velocity is particularly sensitive of this value and suppose a unimodal velocity distribution in the spanwise direction. For this reason, this kind of approach cannot be used in the cross-sections immediately downstream the bridge, where velocities show large spatial variations (see e.g., Figure 4). Herein, the results are presented for cross-section 1, i.e. 50 m upstream of the bridge for the high-flow condition of the 2012 event, and for cross-section 4, i.e. 200 m downstream of the bridge for the modest peak flow condition of the 2022 event, where the effect of bridge piers on the velocity distribution wears off in a shorter distance.

Figure 7 shows the distribution of the surface velocity based on CFD outputs and both the PSD and ESD entropy models. The agreement of both the PSD and the ESD is generally good in the central and the right parts of the channel, and less good in the left part of the channel. Here, due to the irregular bathymetry (i.e., gravel deposit), the 3D-CFD model predicts localized stagnation zones that cannot be captured by the entropy model based on a single value of the surface velocity. This is confirmed by Figure 8a, which shows the cross-sectional distribution of the depth-average velocity and three vertical profiles. In the perspective of estimating the flow discharge, the lateral discrepancies represent a minor limit, as the central part of the cross-sections conveys the largest part of the total discharge.

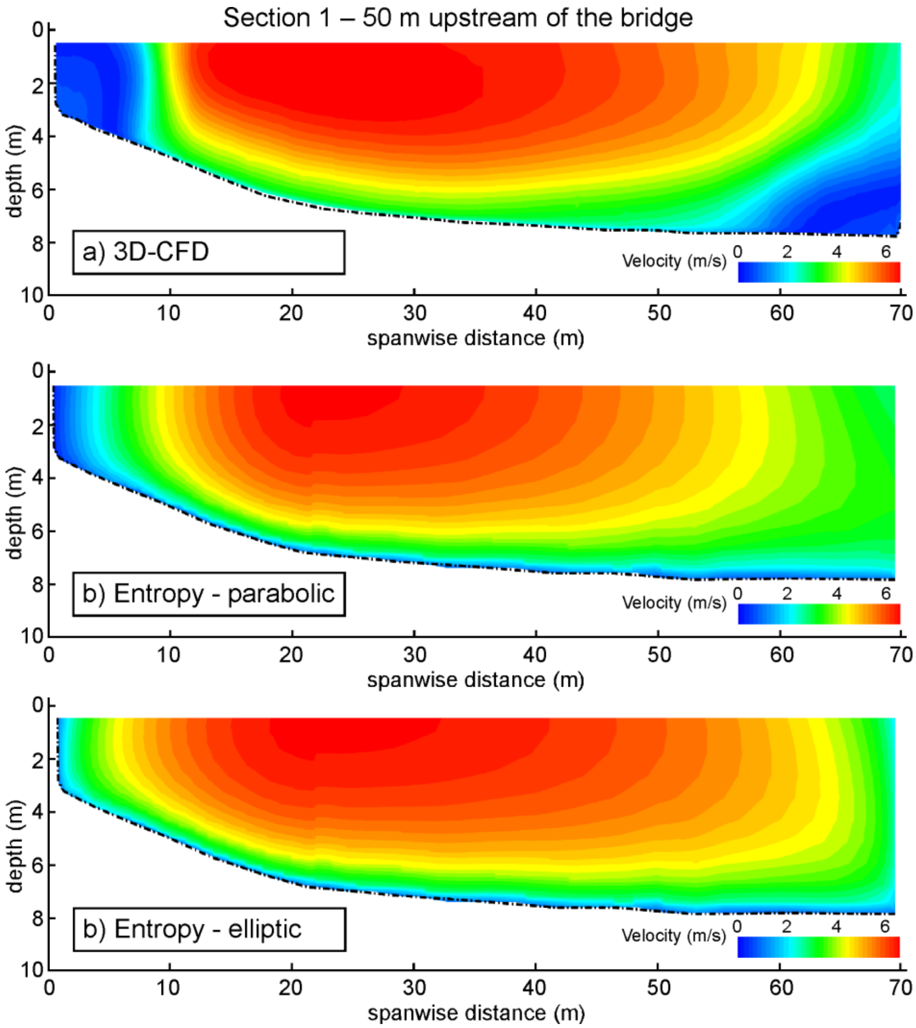

Figure 7. Flood event of 2012, cross-section 1 (50 m upstream of the bridge). Cross-sectional velocity distribution computed with the 3D-CFD model (a), the entropy theory with parabolic (b) and elliptic (c) spanwise velocity distribution.

Overall, the results based on ESD are more accurate than results based on the PSD: they provide similar results at the center of the channel, but the parabolic distribution generally underestimates the flow velocity close to the banks. Both cross-sectional and vertical distributions of the velocity profiles (Figure 7a and Figure 8c) highlight the existence of a velocity dip, i.e. the maximum velocity is below the water surface, particularly at the center of the channel. This is generally the consequence of secondary currents superposed to the main flow (Termini and Moramarco, 2020). Yang et al. (2004) and Moramarco et al. (2017) reported that for large aspect ratios of channel flow, B/D, the dip phenomenon appears primarily near the sidewall region, whereas for relatively low aspect ratios (B/D = 9.26 for cross-section 1) the velocity dip is generally located at the center of the channel (Bahmanpouri et al., 2022b, a; Kundu and Ghoshal, 2018; Moramarco et al., 2017; Termini and Moramarco, 2020). In this case, the 3D flow field from the CFD simulation shows that the dip depends on the

https://doi.org/10.5194/hess-2023-253
Preprint. Discussion started: 14 December 2023

counter-clockwise rotating secondary current generated by the upstream right-handed bend. Indeed, rotational inertia makes these curvature-induced helical flow structures to propagate downstream for relatively long distances (Dominguez Ruben et al., 2021; Lazzarin and Viero, 2023; Thorne et al., 1985).

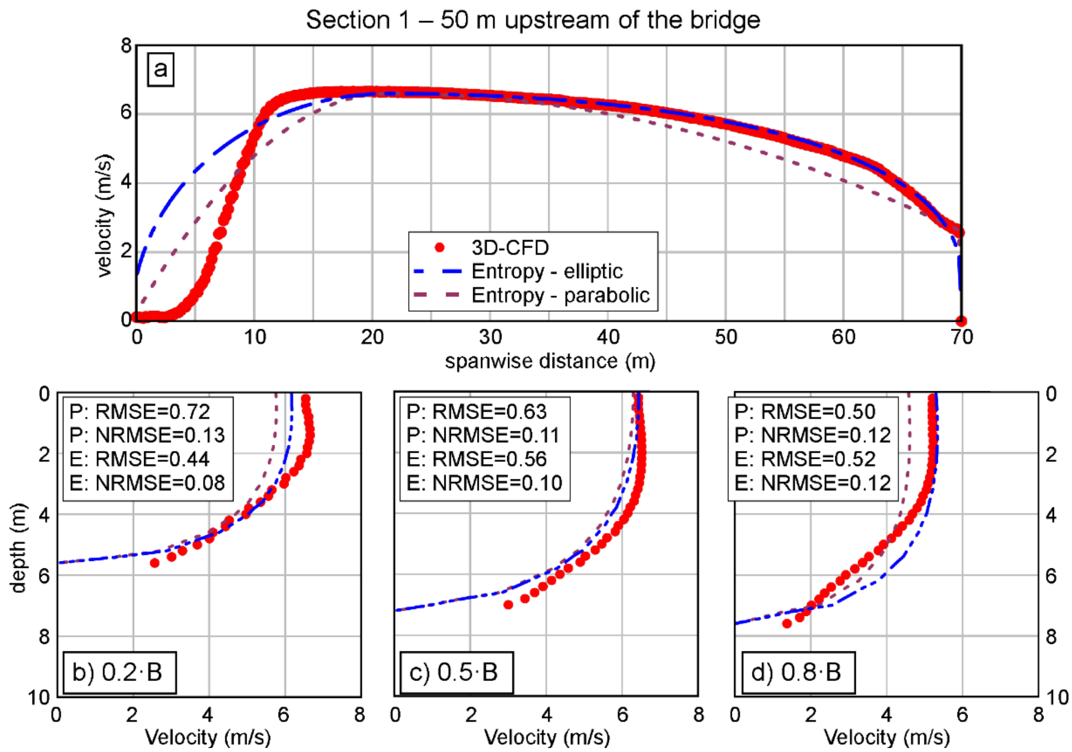

Figure 8. Flood event of 2012, cross-section 1 (50 m upstream of the bridge). Spanwise distribution of the surface velocity (a); comparison of vertical distributions of velocity at 0.2*B* (b), 0.5*B* (c), and 0.8*B* (d).

The distribution of the velocity at the free surface for the cross-section 4 (200 m downstream of the bridge) is presented in Figure 9 for the moderate peak flow condition of the 2022 event. For this cross-section, in the 3D-CFD results (Figure 9a), the maximum surface velocity is located on the left side of the channel, rather than at its center (this aspect is discussed in the following). Forced with the maximum water surface velocity, the entropy model well reproduces the velocity field in the central part of the riverbed. Larger discrepancies are instead observed in the lateral part of the cross-section, with the elliptic spanwise distribution (ESD) that performs slightly better than the parabolic (PSD), particularly in the right side. Figure 10 shows the cross-sectional distribution of the depth-averaged velocity and the velocity distribution along three verticals. In terms of cross-sectional average velocity and flow discharge, both the PSD and ESD produce error that are lower than 10% (Table 4), then quite larger than those obtained using the river-wide surface velocity as input for the entropy model.

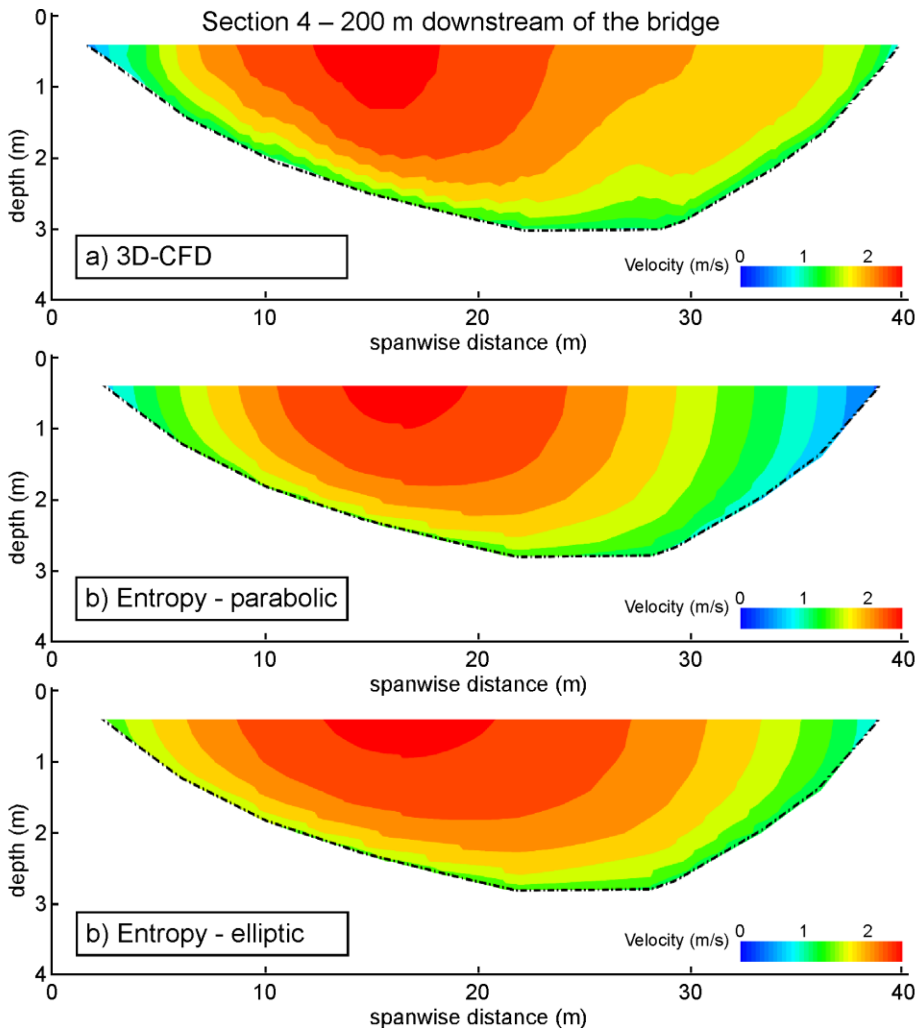

Figure 9. Flood event of 2022, cross-section 4 (200 m downstream of the bridge). Cross-sectional velocity distribution computed with the 3D-CFD model (a), the entropy theory with parabolic (b) and elliptic (c) spanwise velocity distribution.

A last point worth of discussing regards the unusual cross-sectional distribution of flow velocity at section 4 (Figure 9a). The reason why the 3D-CFD model locates the maximum velocity at the left of the talweg is the alternate vortex shedding occurring downstream of the bridge piers, which propagates beyond the last considered cross-section. This is evident in the map of instantaneous surface-velocity of Figure 11. This particular occurrence poses interesting questions on the application of the entropy model to estimate the flow discharge downstream of in-stream structures. First, the spanwise location of the maximum surface velocity is subject to a periodical shift, which prevents its correct detection by means of a fixed sensor with a small-size field of view. Secondly, marked time-varying flow fields, which occasionally (or periodically) deviate from nearly uniform flow conditions, can hardly be captured by any preset velocity distribution. To alleviate the problem, the

https://doi.org/10.5194/hess-2023-253
Preprint. Discussion started: 14 December 2023

periodic signal of surface velocity can be filtered, which is equivalent to look at time-averaged modelled flow fields, which requires knowing the frequency of vortex shedding.

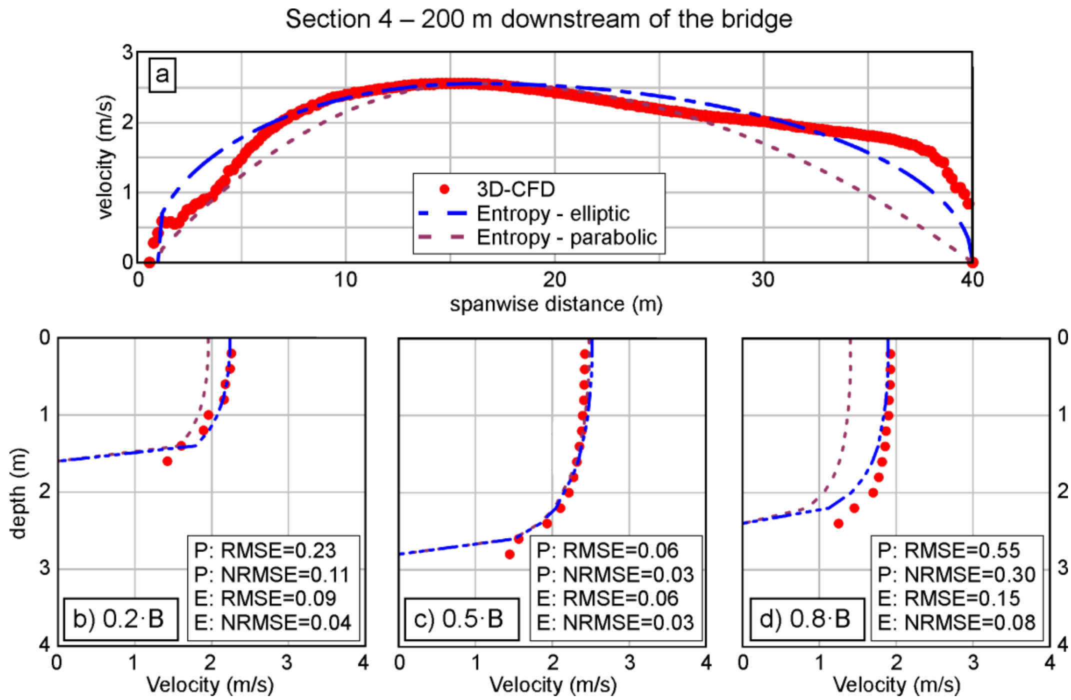

360 **Figure 10. Flood event of 2022, cross-section 4 (200 m downstream of the bridge). Spanwise distribution of the surface velocity (a); comparison of vertical distributions of velocity at 0.2*B* (b), 0.5*B* (c), and 0.8*B* (d).**

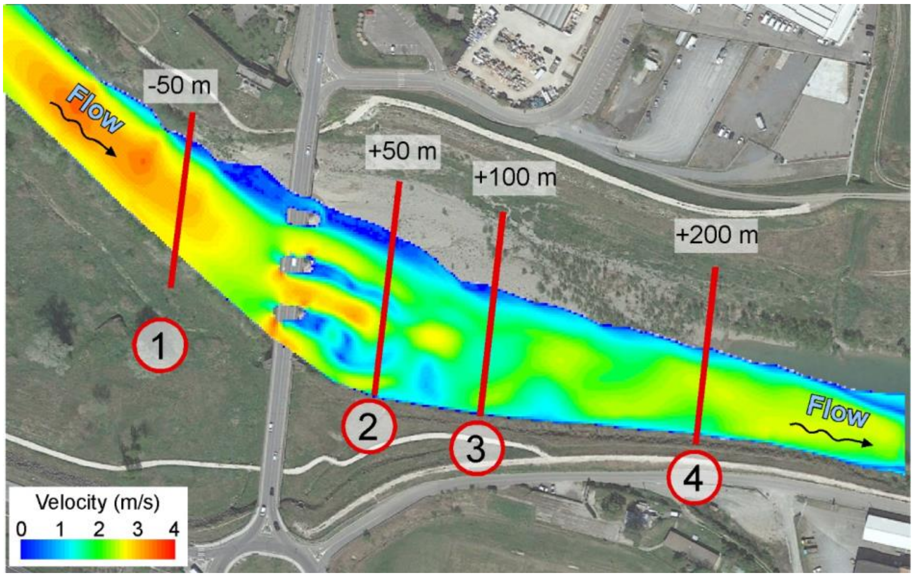

Figure 11. Flood event of 2022. Colormap of the instantaneous surface velocities computed with the 3D-CFD model for the Paglia River at the Adunata bridge (aerial image from © Google Earth).

https://doi.org/10.5194/hess-2023-253
Preprint. Discussion started: 14 December 2023

The results shown in this Section confirm the general accuracy of the entropy model in predicting the velocity distributions. As expected, when using a single value of velocity in place of the river-wide distribution of surface velocity, the precision of the method decreases. Provided that using a single velocity is beyond the scope of the method when the velocity distribution is markedly irregular, the entropy approach can still be forced with a single surface velocity, and produce accurate results, when there are no evidences of strong disturbances of the flow. Indeed, such an approach cannot capture marked unevenness in the flow field, as shown in the case of the lateral low-velocity regions at cross-section 1 for the 2012 event (Figure 7), and in the time-varying flow field of cross-section 4 for the 2022 event (Figure 9).

Distance from the bridge (m) and year	Average velocity (m/s)			Discharge (m³/s)			Error percentage (%)	
	3D-CFD	Entropy		3D-CFD	Entropy			
		Parabolic	Elliptic		Parabolic	Elliptic	Parabolic	Elliptic
−50 (2012)	4.43	4.44	4.83	1’800	1’804	1’962	+0.2	+9.0
−50 (2019)	3.00	3.24	3.40	450	486	510	+8.0	+13.3
−50 (2022)	2.55	2.65	2.74	160	166	172	+3.8	+7.5
+200 (2022)	1.97	1.81	2.02	160	147	164	−8.0	+2.0

Table 4. Comparison between 3D-CFD and entropy-based outputs considering a single surface velocity.

4 Conclusions

The present study investigates the entropy-based cross-sectional distributions of velocity, as well as the associated river discharge, for different flow conditions in a representative case study. As sensors for continuous monitoring of water level and discharge are often mounted on existing bridges, a stretch of the Paglia River is analyzed where a multi-arch bridge with thick piers, which hosts a level gauge and a radar sensor, strongly affects the flow field.

With the goal of assessing the applicability of the entropy model in case of flows disturbed by the presence of in-stream structures, a 3D-CFD model is set up to obtain reliable, physics-based velocity distributions at relevant cross-sections, both upstream and downstream of the bridge. The entropy model is then applied to reproduce this set of velocity distributions, using the modelled surface velocity and the bathymetric data as input.

As a first point, the study highlighted the potential of using accurate, physics-based, 3D-CFD models to deepen the knowledge of river and, specifically, of theoretical methods for discharge estimation. Indeed, 3D-CFD models allows providing pictures of complex flow fields that are more complete than, e.g., ADCP measures, in terms of spatial and temporal distribution and, above all, valid for high-flow regimes which typically prevent any direct measurement of the flow field beneath the free-surface. This entails unexplored chances of outlining best-practices in the use of simplified methods for continuous discharge monitoring, and, as a consequence, to improve their accuracy.

According to the present analysis, the entropy model revealed remarkable skills in reproducing also disturbed and uneven flow fields when the river-wide distribution of the surface velocity is used as input data. This occurred also just downstream of the bridge, where the pier-induced wakes made the velocity distribution multimodal and extremely irregular, with error on

https://doi.org/10.5194/hess-2023-253
Preprint. Discussion started: 14 December 2023

discharge estimates lower than 8%. The availability of innovative measuring techniques, able to collect river-wide surface velocity data at a relatively low cost, adds value to the present findings.

On the other side, the accuracy of the entropy model is reduced when only the maximum surface velocity is used as input data, so that the spanwise velocity distribution has to be assumed on a theoretical basis (e.g., parabolic or elliptical). While such a method is absolutely discouraged in case of disturbed flow fields (e.g., downstream of in-stream structures), it still provides accurate estimates where the velocity field is sufficiently regular.

As a final recommendation, measuring instruments and sensor for surface velocity become more effective when placed upstream of in-stream structures, i.e., where the flow field is only marginally affected by the structure and the velocity distribution is far more regular.

Future research will include the analysis of stage-dependent variations of cross-sectional velocity distribution, particularly in case of compound cross-sections that are typical of natural rivers. More complex scenarios that still need a comprehensive assessment, and which could largely benefit from physics-based numerical modelling, include the case of mobile beds, in which the geometrical variability occurring at the passage of floods adds uncertainty to the discharge estimation.

Appendix A

To impose the boundary conditions to the 3D-CFD model, a 2D depth-averaged model of a longer stretch of the Paglia River has been setup. We used the 2DEF Finite Element model (Defina, 2003; Lazzarin et al., 2023a; Viero, 2019; Viero et al., 2014, 2013), which solves a modified version of the shallow water equations (SWEs) that allow for a robust treatment of wetting and drying over irregular topographies (D'Alpaos and Defina, 2007; Defina, 2000). The SWEs are written as:

$$\begin{aligned} &\eta(h_s)\frac{\partial h_s}{\partial t} + \nabla\cdot\mathbf{q} = 0 \\ &g\nabla h_s + \frac{\mathrm{D}}{\mathrm{D}t}\left(\frac{\mathbf{q}}{Y}\right) + \frac{\boldsymbol{\tau}}{\rho Y} - \nabla\cdot\mathbf{Re} = 0 \end{aligned} \tag{A1}$$

in which h_s is the free surface elevation, t is the time, ∇ and $\nabla\cdot$ denote the 2D gradient and divergence operators, respectively, $\mathbf{q} = (q_x; q_y)$ is the depth-integrated velocity (i.e., the unit-width discharge), Y is the equivalent water depth (i.e., the volume of water per unit area), and $\eta(h_s)$ a storativity coefficient to account for the wetted fraction of the domain, $\boldsymbol{\tau} = (\tau_x; \tau_y)$ is the bed shear stress, evaluated using the Gauckler-Strickler formula, ρ is the water density, and **Re** the horizontal components of the Reynolds stresses, modelled according to the Boussinesq approximation. A mixed Eulerian-Lagrangian approach allows evaluating the total derivative of the flow velocity in the momentum equations using finite differences and a backward tracing technique based on the method of characteristics (Defina, 2003; Giraldo, 2003; Walters and Casulli, 1998). Then, the SWEs are solved with a finite element method, based on triangular, unstructured grids. The model also allows to couple 2D triangular elements with 1D elements (either open- or closed-sections) to model the minor hydraulic network efficiently; other 1D elements are used to model particular devices, such as pumps, weirs, etc. (Martini et al., 2004). The

https://doi.org/10.5194/hess-2023-253
Preprint. Discussion started: 14 December 2023

Hydrology and Earth System Sciences
Discussions

model has been successfully used to simulate flows in various rivers (e.g., Mel et al., 2020a, 2020b; Viero et al., 2019); its effectiveness have been demonstrated also in different research field, such as lagoon and marine environments (e.g., Carniello et al., 2012; Pivato et al., 2020; Tognin et al., 2022; Viero and Defina, 2016).

In the present case, the computational mesh covered a stretch of the Paglia river about 7 km long, from 600 m upstream of the Adunata Bridge to the confluence with the Tiber river, including floodable floodplains (Fig. A1). The average mesh size ranges from 10 m in the riverbed near the Adunata bridge, to 30 m in the floodplains and far downstream of the Adunata bridge. The computational mesh included 61'000 triangular elements, 16 1D elements to simulate underpasses, and 4 1D weir elements to simulate the sill located 500 m downstream of the Adunata Bridge.

The inflow hydrographs, prescribed at the upstream mesh inlet, were derived from water levels measured at the Adunata Bridge using the associated rating curve. At the outlet, an arbitrary rating curve was applied as downstream boundary condition; a sensitivity analysis showed that, because of the distance from the Adunata Bridge, this boundary condition did not produce any perceivable effect in the water levels simulated at the study site.

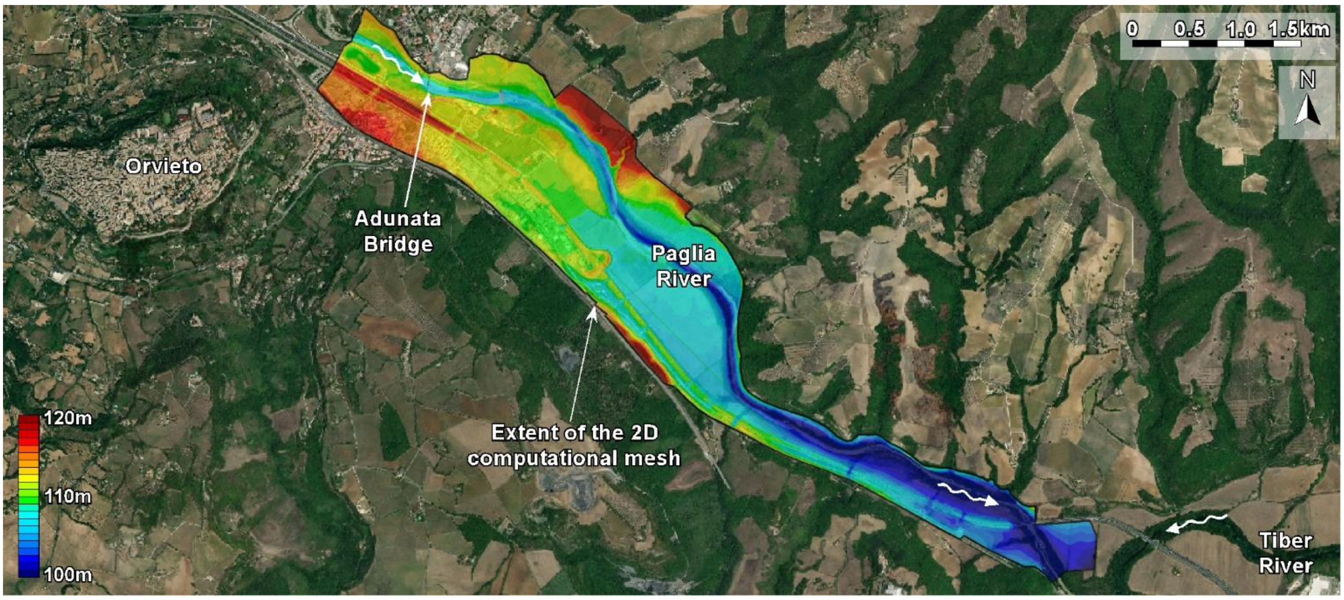

Figure A1. Spatial extent of the 2D computational mesh (aerial image from World Imagery). The color map shows the bottom elevation of the grid elements derived from the LiDAR-based DTM.

Different Gauckler-Strickler coefficients were assigned to the different parts of the domain (e.g., floodplains, densely vegetated areas, etc.) based on the soil cover. The value assigned to the main riverbed were calibrated to match the time series of the water levels measured at the Adunata bridge gauging station for the 2019 flood event (Fig. A2a) and, for the most sever flood event occurred in 2012, the model results were also checked in terms of extent of flooded areas. The minor flood of 2022 was used to verify the model (Fig. A2b). Finally, the depth-averaged velocity just downstream of the Adunata Bridge was compared with the free-surface velocity measured by the radar sensor. Due to the use of a coarse grid and to the

https://doi.org/10.5194/hess-2023-253
Preprint. Discussion started: 14 December 2023

Hydrology and Earth System Sciences
Open Access
EGU
Discussions

depth-average assumption, the 2D model underpredicts the measured water surface systematically (Fig. A2c,d); however, using an amplification factor of 1.7 (gray dots in Fig. A2c,d), the predicted values are quite similar to the measured ones.

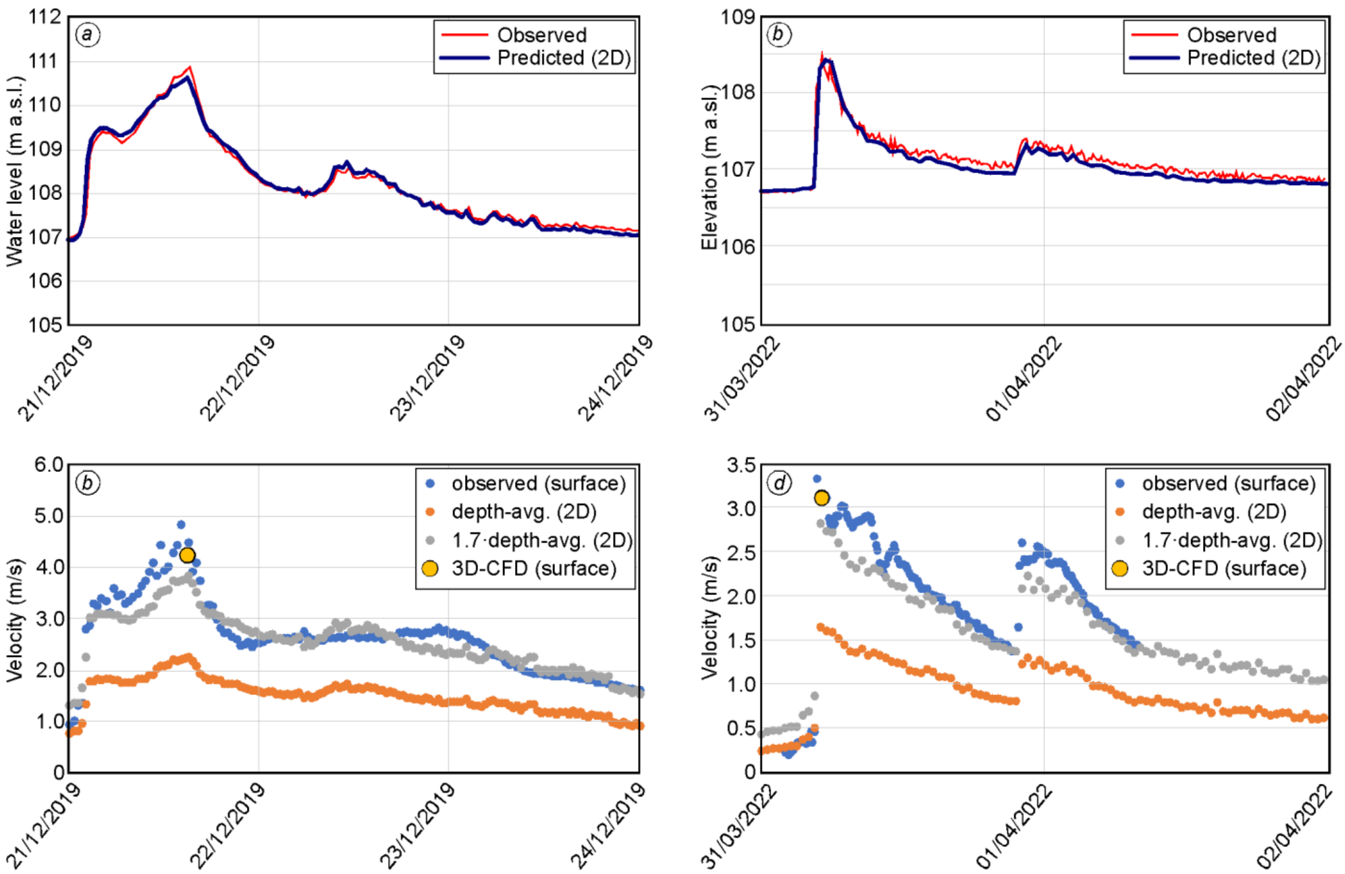

Figure A2. Observed (red) and predicted (blue) water levels at the Adunata Bridge gauging station for the flood events of 2019 (a) and 2022 (b). Observed and predicted water velocity for the flood events of 2019 (c) and 2022 (d).

Data availability

Data available on request from the authors.

Author contribution

Conceptualization: FB, TL, SB, TM, DPV. Formal analysis: FB and TL. Funding acquisition: TM. Investigation: FB and TL. Methodology: FB, TL, SB, TM, DPV. Project administration: SB, TM, DPV. Software: FB, TL, TM, DPV. Supervision: SB, TM, DPV. Visualization FB, TL, DPV. Writing – original draft preparation: FB. Writing – review & editing: TL, SB, TM, DPV.

Competing interests

The authors declare that they have no conflict of interest.

Acknowledgements

This study was supported by Italian National Research Programme PRIN 2017, with the project n. 2017SEB7Z8 "IntEractions between hydrodyNamics and bioTic communities in fluvial Ecosystems: advancement in the knowledge and undeRstanding of PRocesses and ecosystem sustainability by the development of novel technologieS with fIeld monitoriNg and laboratory testing (ENTERPRISING)". T.L. is sponsored by a scholarship provided by the CARIPARO foundation. The authors acknowledge the assistance of Luigi di Micco, Shiva Rezazadeh, and Marco Dionigi.

References

Abdolvandi, A. F., Ziaei, A. N., Moramarco, T., and Singh, V. P.: New approach to computing mean velocity and discharge, Hydrological Sciences Journal, 66, 347–353, https://doi.org/10.1080/02626667.2020.1859115, 2021.

Ammari, A., Bahmanpouri, F., Khelfi, M. E. A., and Moramarco, T.: The regionalizing of the entropy parameter over the north Algerian watersheds: a discharge measurement approach for ungauged river sites, Hydrological Sciences Journal, 67, 1640–1655, https://doi.org/10.1080/02626667.2022.2099744, 2022.

Ataie-Ashtiani, B. and Aslani-Kordkandi, A.: Flow field around side-by-side piers with and without a scour hole, European Journal of Mechanics - B/Fluids, 36, 152–166, https://doi.org/10.1016/j.euromechflu.2012.03.007, 2012.

Bahmanpouri, F., Eltner, A., Barbetta, S., Bertalan, L., and Moramarco, T.: Estimating the Average River Cross-Section Velocity by Observing Only One Surface Velocity Value and Calibrating the Entropic Parameter, Water Resources Research, 58, e2021WR031821, https://doi.org/10.1029/2021WR031821, 2022a.

Bahmanpouri, F., Barbetta, S., Gualtieri, C., Ianniruberto, M., Filizola, N., Termini, D., and Moramarco, T.: Prediction of river discharges at confluences based on Entropy theory and surface-velocity measurements, Journal of Hydrology, 606, 127404, https://doi.org/10.1016/j.jhydrol.2021.127404, 2022b.

Barbetta, S., Camici, S., and Moramarco, T.: A reappraisal of bridge piers scour vulnerability: a case study in the Upper Tiber River basin (central Italy), Journal of Flood Risk Management, 10, 283–300, https://doi.org/10.1111/jfr3.12130, 2017.

Bogning, S., Frappart, F., Blarel, F., Niño, F., Mahé, G., Bricquet, J.-P., Seyler, F., Onguéné, R., Etamé, J., Paiz, M.-C., and Braun, J.-J.: Monitoring Water Levels and Discharges Using Radar Altimetry in an Ungauged River Basin: The Case of the Ogooué, Remote Sensing, 10, https://doi.org/10.3390/rs10020350, 2018.

Bonakdari, H., Larrarte, F., Lassabatere, L., and Joannis, C.: Turbulent velocity profile in fully-developed open channel flows, Environmental Fluid Mechanics, 8, 1–17, https://doi.org/10.1007/s10652-007-9051-6, 2008.

Bonakdari, H., Sheikh, Z., and Tooshmalani, M.: Comparison between Shannon and Tsallis entropies for prediction of shear stress distribution in open channels, Stochastic Environmental Research and Risk Assessment, 29, 1–11, https://doi.org/10.1007/s00477-014-0959-3, 2015.

Briaud, J. L., Chen, H. C., Chang, K. A., Oh, S. J., and Chen, X.: Abutment scour in cohesive materials, NCHRP Report, 24–15(2), Transportation Research Board, National Research Council, Washington, D.C., USA., 2009.

Carniello, L., Defina, A., and D'Alpaos, L.: Modeling sand-mud transport induced by tidal currents and wind waves in shallow microtidal basins: Application to the Venice Lagoon (Italy), Estuarine, Coastal and Shelf Science, 102–103, 105–115, https://doi.org/10.1016/j.ecss.2012.03.016, 2012.

Chahrour, N., Castaings, W., and Barthélemy, E.: Image-based river discharge estimation by merging heterogeneous data with information entropy theory, Flow Measurement and Instrumentation, 81, 102039, https://doi.org/10.1016/j.flowmeasinst.2021.102039, 2021.

Chang, W.-Y., Constantinescu, G., Lien, H.-C., Tsai, W.-F., Lai, J.-S., and Loh, C.-H.: Flow Structure around Bridge Piers of Varying Geometrical Complexity, Journal of Hydraulic Engineering, 139, 812–826, https://doi.org/10.1061/(ASCE)HY.1943-7900.0000742, 2013.

Cheng, Z., Koken, M., and Constantinescu, G.: Approximate methodology to account for effects of coherent structures on sediment entrainment in RANS simulations with a movable bed and applications to pier scour, Advances in Water Resources, 120, 65–82, https://doi.org/10.1016/j.advwatres.2017.05.019, 2018.

Chiu, C.-L.: Velocity Distribution in Open Channel Flow, Journal of Hydraulic Engineering, 115, 576–594, https://doi.org/10.1061/(ASCE)0733-9429(1989)115:5(576), 1989.

Chiu, C.-L. and Said, C. A. A.: Maximum and Mean Velocities and Entropy in Open-Channel Flow, Journal of Hydraulic Engineering, 121, 26–35, https://doi.org/10.1061/(ASCE)0733-9429(1995)121:1(26), 1995.

Chiu, C.-L., Hsu, S.-M., and Tung, N.-C.: Efficient methods of discharge measurements in rivers and streams based on the probability concept, Hydrological Processes, 19, 3935–3946, https://doi.org/10.1002/hyp.5857, 2005.

Constantinescu, G., Koken, M., and Zeng, J.: The structure of turbulent flow in an open channel bend of strong curvature with deformed bed: Insight provided by detached eddy simulation, Water Resources Research, 47, https://doi.org/10.1029/2010WR010114, 2011.

D'Alpaos, L. and Defina, A.: Mathematical modeling of tidal hydrodynamics in shallow lagoons: A review of open issues and applications to the Venice lagoon, Computers & Geosciences, 33, 476–496, https://doi.org/10.1016/j.cageo.2006.07.009, 2007.

Defina, A.: Two-dimensional shallow flow equations for partially dry areas, Water Resources Research, 36, 3251–3264, https://doi.org/10.1029/2000WR900167, 2000.

Defina, A.: Numerical experiments on bar growth, Water Resources Research, 39, 1092, https://doi.org/10.1029/2002WR001455, 2003.

Depetris, P. J.: The Importance of Monitoring River Water Discharge, Frontiers in Water, 3, https://doi.org/10.3389/frwa.2021.745912, 2021.

Di Baldassarre, G. and Montanari, A.: Uncertainty in river discharge observations: a quantitative analysis, Hydrology and Earth System Sciences, 13, 913–921, https://doi.org/10.5194/hess-13-913-2009, 2009.

Dominguez Ruben, L., Szupiany, R. N., Tassi, P., and Vionnet, C. A.: Large meandering bends with high width-to-depth ratios: Insights from hydro-sedimentological processes, Geomorphology, 374, 107521, https://doi.org/10.1016/j.geomorph.2020.107521, 2021.

Dottori, F., Di Baldassarre, G., and Todini, E.: Detailed data is welcome, but with a pinch of salt: Accuracy, precision, and uncertainty in flood inundation modeling, Water Resources Research, 49, 6079–6085, https://doi.org/10.1002/wrcr.20406, 2013.

Ebtehaj, I., Bonakdari, H., Moradi, F., Gharabaghi, B., and Khozani, Z. S.: An integrated framework of Extreme Learning Machines for predicting scour at pile groups in clear water condition, Coastal Engineering, 135, 1–15, https://doi.org/10.1016/j.coastaleng.2017.12.012, 2018.

Eltner, A., Sardemann, H., and Grundmann, J.: Technical Note: Flow velocity and discharge measurement in rivers using terrestrial and unmanned-aerial-vehicle imagery, Hydrology and Earth System Sciences, 24, 1429–1445, https://doi.org/10.5194/hess-24-1429-2020, 2020.

Federico, F., Silvagni, G., and Volpi, F.: Scour Vulnerability of River Bridge Piers, Journal of Geotechnical and Geoenvironmental Engineering, 129, 890–899, https://doi.org/10.1061/(ASCE)1090-0241(2003)129:10(890), 2003.

Fekete, B. M. and Vörösmarty, C. J.: The current status of global river discharge monitoring and potential new technologies complementing traditional discharge measurements, 309, 129–136, 2002.

Fekete, B. M., Looser, U., Pietroniro, A., and Robarts, R. D.: Rationale for Monitoring Discharge on the Ground, Journal of Hydrometeorology, 13, 1977–1986, https://doi.org/10.1175/JHM-D-11-0126.1, 2012.

Franca, M. J., Ferreira, R. M. L., and Lemmin, U.: Parameterization of the logarithmic layer of double-averaged streamwise velocity profiles in gravel-bed river flows, Advances in Water Resources, 31, 915–925, https://doi.org/10.1016/j.advwatres.2008.03.001, 2008.

Fulton, J. and Ostrowski, J.: Measuring real-time streamflow using emerging technologies: Radar, hydroacoustics, and the probability concept, Journal of Hydrology, 357, 1–10, https://doi.org/10.1016/j.jhydrol.2008.03.028, 2008.

Giraldo, F. X.: Strong and weak Lagrange-Galerkin spectral element methods for the shallow water equations, Computers & Mathematics with Applications, 45, 97–121, https://doi.org/10.1016/S0898-1221(03)80010-X, 2003.

Gore, J. A. and Banning, J.: Chapter 3 - Discharge Measurements and Streamflow Analysis, in: Methods in Stream Ecology, Volume 1 (Third Edition), edited by: Hauer, F. R. and Lamberti, G. A., Academic Press, Boston, 49–70, https://doi.org/10.1016/B978-0-12-416558-8.00003-2, 2017.

Guo, J.: Modified log-wake-law for smooth rectangular open channel flow, Journal of Hydraulic Research, 52, 121–128, https://doi.org/10.1080/00221686.2013.818584, 2014.

Herschy, R. W.: Streamflow Measurement (3rd ed.), CRC Press, https://doi.org/10.1201/9781482265880, 2009.

Hirt, C. W. and Nichols, B. D.: Volume of fluid (VOF) method for the dynamics of free boundaries, Journal of Computational Physics, 39, 201–225, https://doi.org/10.1016/0021-9991(81)90145-5, 1981.

Horna-Munoz, D. and Constantinescu, G.: A fully 3-D numerical model to predict flood wave propagation and assess efficiency of flood protection measures, Advances in Water Resources, 122, 148–165, https://doi.org/10.1016/j.advwatres.2018.10.014, 2018.

https://doi.org/10.5194/hess-2023-253
Preprint. Discussion started: 14 December 2023

Hydrology and Earth System Sciences
Open Access
Discussions

Jodeau, M., Hauet, A., Paquier, A., Le Coz, J., and Dramais, G.: Application and evaluation of LS-PIV technique for the monitoring of river surface velocities in high flow conditions, Flow Measurement and Instrumentation, 19, 117–127, https://doi.org/10.1016/j.flowmeasinst.2007.11.004, 2008.

Kästner, K., Hoitink, A. J. F., Torfs, P. J. J. F., Vermeulen, B., Ningsih, N. S., and Pramulya, M.: Prerequisites for Accurate Monitoring of River Discharge Based on Fixed-Location Velocity Measurements, Water Resources Research, 54, 1058–1076, https://doi.org/10.1002/2017WR020990, 2018.

Khosronejad, A., Kang, S., and Sotiropoulos, F.: Experimental and computational investigation of local scour around bridge piers, Advances in Water Resources, 37, 73–85, https://doi.org/10.1016/j.advwatres.2011.09.013, 2012.

Kirkil, G. and Constantinescu, G.: Effects of cylinder Reynolds number on the turbulent horseshoe vortex system and near wake of a surface-mounted circular cylinder, Physics of Fluids, 27, 075102, https://doi.org/10.1063/1.4923063, 2015.

Kundu, S. and Ghoshal, K.: An Entropy Based Model for Velocity-Dip-Position, Journal of Environmental Informatics, 33, 113–128, 2018.

Laursen, E. M.: Scour at Bridge Crossings, Journal of the Hydraulics Division, 86, 39–54, https://doi.org/10.1061/JYCEAJ.0000426, 1960.

Laursen, E. M.: An Analysis of Relief Bridge Scour, Journal of the Hydraulics Division, 89, 93–118, https://doi.org/10.1061/JYCEAJ.0000896, 1963.

Lazzarin, T. and Viero, D. P.: Curvature-induced secondary flow in 2D depth-averaged hydro-morphodynamic models: An assessment of different approaches and key factors, Advances in Water Resources, 171, 104355, https://doi.org/10.1016/j.advwatres.2022.104355, 2023.

Lazzarin, T., Defina, A., and Viero, D. P.: Assessing 40 Years of Flood Risk Evolution at the Micro-Scale Using an Innovative Modeling Approach: The Effects of Urbanization and Land Planning, Geosciences, 13, https://doi.org/10.3390/geosciences13040112, 2023a.

Lazzarin, T., Viero, D. P., Defina, A., and Cozzolino, L.: Flow under vertical sluice gates: Flow stability at large gate opening and disambiguation of partial dam-break multiple solutions, Physics of Fluids, 35, 024114, https://doi.org/10.1063/5.0131953, 2023b.

Li, B. and Zhang, X.: Evolution of outer bank cell in open-channel bends, Environmental Fluid Mechanics, 22, 715–742, https://doi.org/10.1007/s10652-022-09865-2, 2022.

Lu, B., Petukhov, V., Zhang, M., Wang, X., Yue, S., Zhou, H., Kholodov, A., and Yu, G.: Prediction of flow-induced local scour depth at the uniform bridge pier using masked attention neural network, Ocean Engineering, 266, 113018, https://doi.org/10.1016/j.oceaneng.2022.113018, 2022.

Luo, H., Fytanidis, D. K., Schmidt, A. R., and García, M. H.: Comparative 1D and 3D numerical investigation of open-channel junction flows and energy losses, Advances in Water Resources, 117, 120–139, https://doi.org/10.1016/j.advwatres.2018.05.012, 2018.

Martini, P., Carniello, L., and Avanzi, C.: Two dimensional modelling of flood flows and suspended sedimenttransport: the case of the Brenta River, Veneto (Italy), Natural Hazards and Earth System Sciences, 4, 165–181, https://doi.org/10.5194/nhess-4-165-2004, 2004.

Meals, D. W. and Dressing, S. A.: Surface water flow measurement for water quality monitoring projects, 2008.

Mel, R. A., Viero, D. P., Carniello, L., and D'Alpaos, L.: Multipurpose Use of Artificial Channel Networks for Flood Risk Reduction: The Case of the Waterway Padova–Venice (Italy), Water, 12, https://doi.org/10.3390/w12061609, 2020a.

Mel, R. A., Viero, D. P., Carniello, L., and D'Alpaos, L.: Optimal floodgate operation for river flood management: The case study of Padova (Italy), Journal of Hydrology: Regional Studies, 30, 100702, https://doi.org/10.1016/j.ejrh.2020.100702, 2020b.

Moramarco, T. and Singh, V. P.: Formulation of the Entropy Parameter Based on Hydraulic and Geometric Characteristics of River Cross Sections, Journal of Hydrologic Engineering, 15, 852–858, https://doi.org/10.1061/(ASCE)HE.1943-5584.0000255, 2010.

Moramarco, T., Saltalippi, C., and Singh, V. P.: Estimation of Mean Velocity in Natural Channels Based on Chiu's Velocity Distribution Equation, Journal of Hydrologic Engineering, 9, 42–50, https://doi.org/10.1061/(ASCE)1084-0699(2004)9:1(42), 2004.

Moramarco, T., Barbetta, S., and Tarpanelli, A.: From Surface Flow Velocity Measurements to Discharge Assessment by the Entropy Theory, Water, 9, https://doi.org/10.3390/w9020120, 2017.

Nezu, I. and Nakagawa, H.: Turbulence in Open Channel Flows, Balkema., Rotterdam, The Netherlands, 1993.

Nikora, V. and Roy, A. G.: Secondary Flows in Rivers: Theoretical Framework, Recent Advances, and Current Challenges, in: Gravel-Bed Rivers, John Wiley & Sons, Ltd, 1–22, https://doi.org/10.1002/9781119952497.ch1, 2011.

Pivato, M., Carniello, L., Viero, D. P., Soranzo, C., Defina, A., and Silvestri, S.: Remote Sensing for Optimal Estimation of Water Temperature Dynamics in Shallow Tidal Environments, Remote Sensing, 12, https://doi.org/10.3390/rs12010051, 2020.

Proust, S. and Nikora, V. I.: Compound open-channel flows: effects of transverse currents on the flow structure, Journal of Fluid Mechanics, 885, A24, https://doi.org/10.1017/jfm.2019.973, 2020.

Salaheldin, T. M., Imran, J., and Chaudhry, M. H.: Numerical Modeling of Three-Dimensional Flow Field Around Circular Piers, Journal of Hydraulic Engineering, 130, 91–100, https://doi.org/10.1061/(ASCE)0733-9429(2004)130:2(91), 2004.

Schweitzer, S. A. and Cowen, E. A.: Instantaneous River-Wide Water Surface Velocity Field Measurements at Centimeter Scales Using Infrared Quantitative Image Velocimetry, Water Resources Research, 57, e2020WR029279, https://doi.org/10.1029/2020WR029279, 2021.

Shih, T.-H., Liou, W. W., Shabbir, A., Yang, Z., and Zhu, J.: A new k-ϵ eddy viscosity model for high reynolds number turbulent flows, Computers & Fluids, 24, 227–238, https://doi.org/10.1016/0045-7930(94)00032-T, 1995.

Singh, V. P., Sivakumar, B., and Cui, H.: Tsallis Entropy Theory for Modeling in Water Engineering: A Review, Entropy, 19, https://doi.org/10.3390/e19120641, 2017.

Spada, E., Sinagra, M., Tucciarelli, T., and Biondi, D.: Unsteady State Water Level Analysis for Discharge Hydrograph Estimation in Rivers with Torrential Regime: The Case Study of the February 2016 Flood Event in the Crati River, South Italy, Water, 9, https://doi.org/10.3390/w9040288, 2017.

https://doi.org/10.5194/hess-2023-253
Preprint. Discussion started: 14 December 2023

Sterling, M. and Knight, D.: An attempt at using the entropy approach to predict the transverse distribution of boundary shear stress in open channel flow, Stochastic Environmental Research and Risk Assessment, 16, 127–142, https://doi.org/10.1007/s00477-002-0088-2, 2002.

Sumer, B. M., Christiansen, N., and Fredsøe, J.: The horseshoe vortex and vortex shedding around a vertical wall-mounted cylinder exposed to waves, Journal of Fluid Mechanics, 332, 41–70, https://doi.org/10.1017/S0022112096003898, 1997.

Termini, D. and Moramarco, T.: Application of entropic approach to estimate the mean flow velocity and Manning roughness coefficient in a high-curvature flume, Hydrology Research, 48, 634–645, https://doi.org/10.2166/nh.2016.106, 2017.

Termini, D. and Moramarco, T.: Entropic model application to identify cross-sectional flow effect on velocity distribution in a large amplitude meandering channel, Advances in Water Resources, 143, 103678, https://doi.org/10.1016/j.advwatres.2020.103678, 2020.

Thorne, C. R., Zevenbergen, L. W., Pitlick, J. C., Rais, S., Bradley, J. B., and Julien, P. Y.: Direct measurements of secondary currents in a meandering sand-bed river, Nature, 315, 746–747, https://doi.org/10.1038/315746a0, 1985.

Tognin, D., Finotello, A., D'Alpaos, A., Viero, D. P., Pivato, M., Mel, R. A., Defina, A., Bertuzzo, E., Marani, M., and Carniello, L.: Loss of geomorphic diversity in shallow tidal embayments promoted by storm-surge barriers, Science Advances, 8, eabm8446, https://doi.org/10.1126/sciadv.abm8446, 2022.

Vandaele, R., Dance, S. L., and Ojha, V.: Calibrated river-level estimation from river cameras using convolutional neural networks, Environmental Data Science, 2, e11, https://doi.org/10.1017/eds.2023.6, 2023.

Viero, D. P.: Modelling urban floods using a finite element staggered scheme with an anisotropic dual porosity model, Journal of Hydrology, 568, 247–259, https://doi.org/10.1016/j.jhydrol.2018.10.055, 2019.

Viero, D. P. and Defina, A.: Water age, exposure time, and local flushing time in semi-enclosed, tidal basins with negligible freshwater inflow, Journal of Marine Systems, 156, 16–29, https://doi.org/10.1016/j.jmarsys.2015.11.006, 2016.

Viero, D. P., D'Alpaos, A., Carniello, L., and Defina, A.: Mathematical modeling of flooding due to river bank failure, Advances in Water Resources, 59, 82–94, https://doi.org/10.1016/j.advwatres.2013.05.011, 2013.

Viero, D. P., Peruzzo, P., Carniello, L., and Defina, A.: Integrated mathematical modeling of hydrological and hydrodynamic response to rainfall events in rural lowland catchments, Water Resources Research, 50, 5941–5957, https://doi.org/10.1002/2013WR014293, 2014.

Viero, D. P., Roder, G., Matticchio, B., Defina, A., and Tarolli, P.: Floods, landscape modifications and population dynamics in anthropogenic coastal lowlands: The Polesine (northern Italy) case study, Science of The Total Environment, 651, 1435–1450, https://doi.org/10.1016/j.scitotenv.2018.09.121, 2019.

Vyas, J. K., Perumal, M., and Moramarco, T.: Entropy Based River Discharge Estimation Using One-Point Velocity Measurement at 0.6D, Water Resources Research, 57, e2021WR029825, https://doi.org/10.1029/2021WR029825, 2021.

Walters, R. A. and Casulli, V.: A robust, finite element model for hydrostatic surface water flows, Communications in Numerical Methods in Engineering, 14, 931–940, https://doi.org/10.1002/(SICI)1099-0887(1998100)14:10<931::AID-CNM199>3.0.CO;2-X, 1998.

https://doi.org/10.5194/hess-2023-253
Preprint. Discussion started: 14 December 2023

Hydrology and Earth System Sciences Discussions

Yang, S.-Q., Tan, S.-K., and Lim, S.-Y.: Velocity Distribution and Dip-Phenomenon in Smooth Uniform Open Channel Flows, Journal of Hydraulic Engineering, 130, 1179–1186, https://doi.org/10.1061/(ASCE)0733-9429(2004)130:12(1179), 2004.

Yang, S.-Q., Tan, S. K., and Wang, X.-K.: Mechanism of secondary currents in open channel flows, Journal of Geophysical Research: Earth Surface, 117, https://doi.org/10.1029/2012JF002510, 2012.

Yang, Y., Xiong, X., Melville, B. W., and Sturm, T. W.: Flow Redistribution at Bridge Contractions in Compound Channel for Extreme Hydrological Events and Implications for Sediment Scour, Journal of Hydraulic Engineering, 147, 04021005, https://doi.org/10.1061/(ASCE)HY.1943-7900.0001861, 2021.

Yoshimura, H. and Fujita, I.: Investigation of free-surface dynamics in an open-channel flow, Journal of Hydraulic Research, 58, 231–247, https://doi.org/10.1080/00221686.2018.1561531, 2020.

Zhang, Z., Zhou, Y., Liu, H., and Gao, H.: In-situ water level measurement using NIR-imaging video camera, Flow Measurement and Instrumentation, 67, 95–106, https://doi.org/10.1016/j.flowmeasinst.2019.04.004, 2019.